X-ray fluorescence from a model liquid/liquid solvent extraction system

Wei Bu,[1,a)] Binyang Hou,[1] Miroslav Mihaylov,[1] Ivan Kuzmenko,[2] Binhua Lin,[3] Mati Meron,[3] L. Soderholm,[4] Guangming Luo,[4] and Mark L. Schlossman[1,a)]
[1]*Department of Physics, University of Illinois at Chicago, Chicago, Illinois 60607, USA*
[2]*XSD, Advanced Photon Source, Argonne National Laboratory, Argonne, Illinois 60439, USA*
[3]*The Center for Advanced Radiation Sources, University of Chicago, Chicago, Illinois 60637, USA*
[4]*Chemical Sciences and Engineering Division, Argonne National Laboratory, Argonne, Illinois 60439, USA*

(Received 15 October 2010; accepted 17 March 2011; published online 30 November 2011)

X-ray fluorescence near total reflection (XFNTR) is measured from the liquid/liquid interface between dodecane and an $ErCl_3$ aqueous solution by monitoring L shell Er emission lines. A custom sample cell is used to minimize absorption of the fluorescence x-rays that pass through dodecane on their way to the detector. The Er^{3+} concentration near the interface is related to the fluorescence intensity by a scale factor that is extracted by fitting the incident-angle dependent Er $L\alpha$ emission line intensities for different $ErCl_3$ bulk concentrations. As an application, we present the use of XFNTR to monitor the growth of interfacial crud in a model solvent extraction system consisting of an interface between a dodecane solution of bis(2-ethylhexyl) phosphate (HDEHP) and an $ErCl_3$ aqueous solution. © *2011 American Institute of Physics*. [doi:10.1063/1.3661983]

I. INTRODUCTION

The interface between two immiscible liquids such as water and oil is of scientific interest because of its relevance to various scientific and industrial applications such as solvent extraction, drug transport, and phase transfer catalysis.[1] The fundamental aspects of the interfacial structure on the molecular length scale that are relevant for these processes are unknown. This ignorance is primarily due to a lack of suitable experimental techniques that probe the structure of buried liquid/liquid interfaces. Nonlinear optical techniques such as second harmonic generation,[2–4] sum frequency generation,[5,6] and potential-modulated spectroscopy,[7,8] are commonly used to probe this interface by taking advantage of the fact that the signal is produced mainly by molecules in the interfacial region. Recently, synchrotron x-ray and neutron surface scattering techniques such as reflectivity and off-specular diffuse scattering, among others, have become useful tools to study liquid/liquid interfaces. They have been used successfully in the study of interfacial width,[9–11] monolayer and nanoparticle structure,[12–14] and ionic distributions near the interface.[15] However, these non-resonant scattering techniques probe the electron or scattering length density and cannot directly identify the distribution of specific elements at the interface.

Liquid-liquid extraction is a chemical method used to separate a targeted solution species from a mixture. It is used in a broad range of applications from heavy oil recovery at the reservoir to the purification of vegetable oils to uranium separations for nuclear energy purposes. For metal-ion applications the technique generally involves the isolation of a specific ion from an aqueous solution via transport into an organic phase, often with the assistance of an extractant molecule as a solubilizing agent. Whereas this biphasic separation is driven by small differences in thermodynamic stabilities between the metal-complexes that form in the two solutions, the rate and ultimate efficacy of a separation is often governed by the complex physico-chemical properties of the interface.[16] Although interfacial phenomena are understood to play a critical role in separations, the interdisciplinary nature of the subject combined with the absence of experiments targeting metal speciation and the structure of aqueous, organic, and extractant complexes at the interface have left this important component of solvent extraction largely unexplored. Their determination remains an open challenge.

X-ray fluorescence near total reflection (XFNTR), first introduced by Bloch *et al.*,[17,18] has been widely used on liquid/vapor interfaces[17–22] but seldom on liquid/liquid interfaces.[23] However, it could be a useful technique to study the interfacial mechanisms in solvent extraction processes because it involves a single-ion spectroscopic technique that is highly selective for metal ions and their speciation at interfaces. In this article, we report a detailed determination of Er L shell fluorescence spectra from interfaces between dodecane and aqueous solutions of $ErCl_3$ at different wave vector transfers, $Q_z = 2k_0 \sin\alpha$ (k_0 and α are the x-ray wave number and incident angle, respectively). This aqueous/organic system, combined with bis(2-ethylhexyl) phosphate (HDEHP) as an extractant, is part of an ongoing study undertaken to address questions on how to understand and improve actinide/lanthanide separations, which are important to the nuclear community.[24,25] On a practical note, our measurements included the study of interfacial "cruds" that are known to plague liquid/liquid extractions such as those in the dodecane(HDEHP)/water($ErCl_3$) solvent-extraction system.

II. EXPERIMENTAL SETUP AND METHODS

A. Materials

In this study, we selected dodecane ($CH_3(CH_2)_{10}CH_3$) as the organic solvent because it is commonly used in

[a)]Authors to whom correspondence should be addressed. Electronic addresses: weibu@uic.edu and schloss@uic.edu.

industrial solvent extraction. The dodecane was purchased from Sigma-Aldrich (>99% purity) and further purified by passing it six times through activated alumina in a chromatography column.[26] The extractant, bis(2-ethylhexyl) phosphate (HDEHP; >97%), was purchased from Sigma-Aldrich, purified by the copper bis(2-ethylhexyl) phosphate precipitation method,[27] and dissolved in dodecane for use in the crud preparation experiment.

Erbium chloride hexahydrate ($ErCl_3 \cdot 6H_2O$; >99.99%) was purchased from Alfa-Aesar and further purified by filtering a concentrated solution (1 M) through omnipore membrane paper in order to remove surface-active impurities. This solution was placed in contact with purified dodecane in a separation funnel for several hours, then drained from the funnel and used as the stock solution for the preparation of lower concentration aqueous solutions of $ErCl_3$. Ultrapure water (produced by a Nanopure UV Barnstead system) was used for all aqueous solution preparations. The *p*H values of all aqueous solutions are adjusted to *p*H 3 by hydrochloric acid (Fisher Scientific; trace metal grade) in order to mimic conditions of efficient extraction, while avoiding interfacial precipitation in the samples with HDEHP. Dodecane/water ($ErCl_3$) interfaces were tested for the presence of surface-active components by monitoring the interfacial tension (measured with a Wilhelmy plate) over a period of several hours after the interfaces were formed. The tension was constant to within 0.15 mN/m during this time, which indicated the high purity of the materials.[26]

B. Sample cell

Figure 1 is a schematic of the sample cell used for the x-ray measurements. The glass tray is cleaned in a sulfuric acid solution of ammonium persulfate (18 g/L) to render it hydrophilic. However, the top edge of the glass tray is rendered effectively hydrophobic by roughening it with a grinder during the manufacturing process and then wetting it by drops of dodecane prior to filling the tray with water. The inside corner of this top edge pins the water/dodecane interface. Adjusting the volume of the aqueous solution with a syringe and leveling the cell along axes parallel and perpendicular to the incident x-ray beam produces a very flat interface. With adequate sample flatness the x-ray reflectivity is constant as the x-ray beam is scanned across the interface at a fixed incident angle. The interfacial area, determined by the glass tray dimension, is 80 mm × 60 mm (along the beam × transverse).

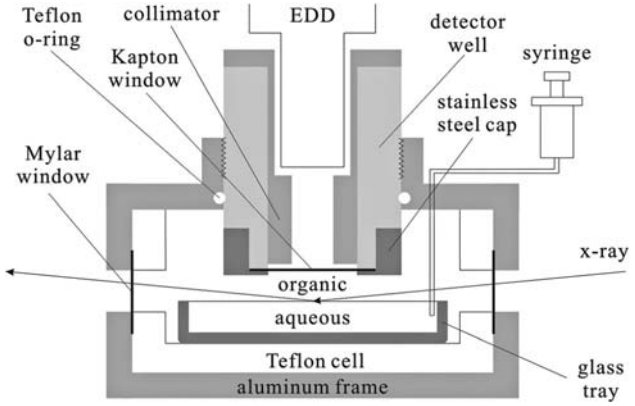

FIG. 1. Cross-sectional view of the sample cell to scale. EDD refers to the energy dispersive detector. The three windows are sealed with Teflon-coated o-rings to ensure that the sample cell is leak-tight.

A Vortex-EX® multicathode x-ray detector (SII Nano Technology USA, Inc.) is used as the energy dispersive detector (EDD). It is placed in the cylindrical well of the sample cell (see Fig. 1). Fluorescent x-rays from the sample pass through a thin layer of dodecane, then through a thin Kapton window (126 μm) that separates the dodecane from air in the cylindrical well. The fluorescence intensity from the interface is reduced by absorption in the dodecane. The thickness of the layer of dodecane between the dodecane/water interface and the Kapton window can be reduced to about 1.5 mm by rotating the detector well. This thickness is close to the dodecane attenuation length of 1.1 mm for the Er $L\beta_1$ emission line at 7.811 keV.

A cylindrical collimator (6.35 mm inside radius and 25.4 mm in length) that is situated in the well between the Kapton window and the detector determines the effective detection area, i.e., the projection of the active area of the detector (4 mm radius) onto the sample, to be a circle with a radius of 7 mm. The effective detection area is smaller than the incident beam footprint on the interface for all values of Q_z used in this study, making a footprint correction unnecessary for the data analysis.

C. X-ray method

X-ray fluorescence measurements were conducted at beamlines 15-ID and 9-ID at the Advanced Photon Source (Argonne National Laboratory, USA) with a liquid surface instrument described in detail elsewhere.[28] The highly monochromatic x-ray beam (20 keV; $\lambda = 0.61992$ Å) passes through the upper organic phase to reflect off the dodecane/water interface. An advantage of the fluorescence technique is that it can identify the contribution from a specific ion by its characteristic fluorescence spectrum. Since the x-ray penetration depth changes dramatically around the critical angle for total reflection, the fluorescence signals below and above the critical angle are dominated by the interface and the bulk, respectively.

III. RESULTS AND DISCUSSION

A. Dodecane/water ($ErCl_3$) interfaces

Figure 2 shows the x-ray fluorescence spectra for the dodecane/water (0.4 M $ErCl_3$) interface below ($Q_z = 0.008$ Å^{-1}; circles) and above ($Q_z = 0.018$ Å^{-1}; squares) the critical angle for total reflection (at $Q_z = 0.0118$ Å^{-1}), and the fluorescence spectrum at $Q_z = 0$ Å^{-1} (triangles) that is measured with the incident beam passing through the upper phase, slightly above and parallel to the interface. The intensity shown in Fig. 2 is the absolute fluorescence intensity, I_f, normalized to the intensity, I_0, recorded by a monitor of the incident beam flux, which is located upstream of the sample cell. All main emission lines from the Er *L* shell are identified as shown in Fig. 2. The label $L\alpha$ refers to the two emission lines $L\alpha_1$ and $L\alpha_2$, whose energy separation (43.7 eV) is smaller

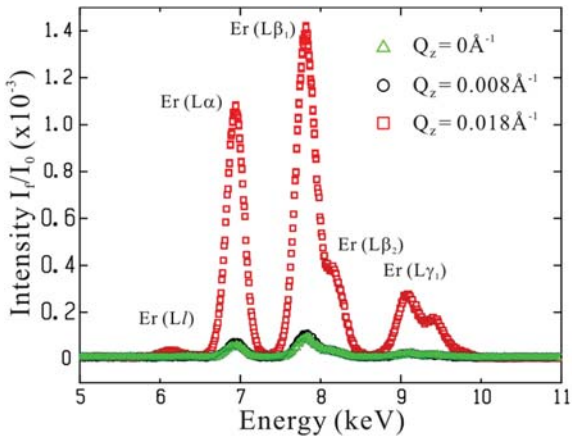

FIG. 2. (Color online) Normalized fluorescence spectra from the dodecane/water (0.4 M $ErCl_3$) (*p*H 3) interface at different incident wave vector transfers, Q_z as indicated. Error bars are smaller than the symbols.

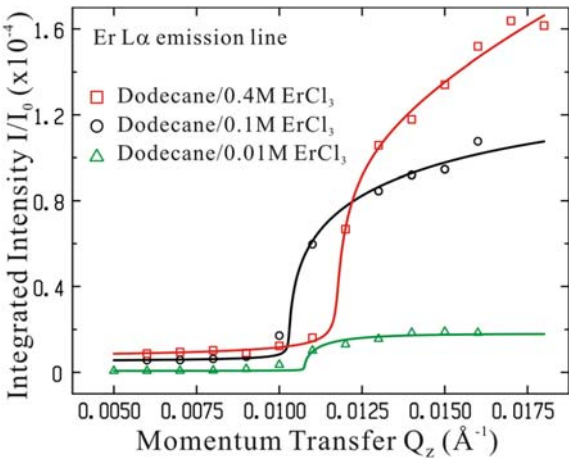

FIG. 3. (Color online) Er $L\alpha$ emission line intensity vs the momentum transfer, Q_z for the dodecane/water (X M $ErCl_3$) interface with $X = 0.01$ M (triangles), $X = 0.1$ M (circles), and $X = 0.4$ M (squares). Solid lines are the fits described in the text. Error bars are smaller than the symbols.

than the detector resolution (~136 eV) and are therefore indistinguishable.

The fluorescence intensity in Fig. 2 shows a significant enhancement from low to high Q_z, which is due primarily to the change in x-ray penetration depth. However, the observed ratio of the intensities of the measurements at high to low Q_z is substantially smaller than the ratio of the penetration depths at $Q_z = 0.018$ Å^{-1} (1.5 μm) to $Q_z = 0.008$ Å^{-1} (12 nm). The substantially enhanced fluorescence at low Q_z is the result of a secondary scattering process in which x-rays from the incident and reflected beams are scattered first from dodecane in the top phase, then penetrate into the lower aqueous phase to produce additional fluorescence from ions in that phase. Figure 2 shows that the Er fluorescence spectrum produced by an x-ray beam that passes through only the top phase ($Q_z = 0$ Å^{-1} in Fig. 2), but very close to the interface, has an intensity similar to the fluorescence produced by the reflection below the critical angle at $Q_z = 0.008$ Å^{-1}. Therefore, the secondary scattering dominates the fluorescence signal below the critical angle. Similar measurements that use an x-ray beam transmitted through only the top phase (also at $Q_z = 0$ Å^{-1}), but with the beam further from the interface show a slightly reduced effect, which is consistent with our expectation that the concentration of Er^{3+} ions in the dodecane top phase is negligible under these conditions.

Another feature in the spectra that is due to the presence of the upper phase is worth mentioning. The $L\alpha$ line has a lower intensity than $L\beta_1$ in Fig. 2 even though the relative intensities from an isolated Er atom would be reversed. This effect is the result of a larger absorption of the lower energy fluorescence signal by the upper phase.

Figure 3 illustrates the variation of integrated fluorescence intensity of the Er $L\alpha$ emission line with momentum transfer, Q_z, for the interface between dodecane and aqueous solutions of $ErCl_3$ at three different concentrations. The integrated $L\alpha$ emission line intensity, I/I_0, is represented by the product of the Gaussian peak intensity and width from fitting the spectra in Fig. 2 to Gaussian peak shapes. All three data sets exhibit a similar sharp transition around the critical angle, which varies with the $ErCl_3$ bulk concentration ($Q_c = 0.0104$, 0.0107, and 0.0118 Å^{-1} for 0.01, 0.1, and 0.4 M $ErCl_3$, respectively). The critical momentum transfer is calculated by $Q_c = 4\sqrt{\pi r_e(\rho_{aq} - \rho_{oil})}$, where $r_e = 2.818 \times 10^{-13}$ cm is the classical electron radius, ρ_{aq} is the electron density of the aqueous phase (0.3341, 0.3392, and 0.3560 e^- Å^{-3} for 0.01, 0.1, and 0.4 M $ErCl_3$, respectively), and $\rho_{oil} = 0.2854$ e^- Å^{-3} is the electron density of the oil phase.

Calculation of the fluorescence intensity requires a careful consideration of the scattering geometry. The intensity of the x-ray beam below the interface, $I(x, z, \alpha)$, is determined by the position (x, z) and the incident angle, α, in the geometry illustrated in Fig. 4. If the intensity at the center of the interface, $I(0, 0)$, is normalized to unity, then

$$\frac{I(x, z, \alpha)}{I(0, 0)} = T(\alpha)e^{-z/\Lambda_w(\alpha)}e^{\mu_0 z/\alpha}e^{-\mu_0 x}, \quad (1)$$

where $T(\alpha)$ is the Fresnel transmission, $\Lambda_w(\alpha)$ is the penetration depth of the bottom phase which depends on the salt concentration, and μ_0 is the absorption coefficient of the

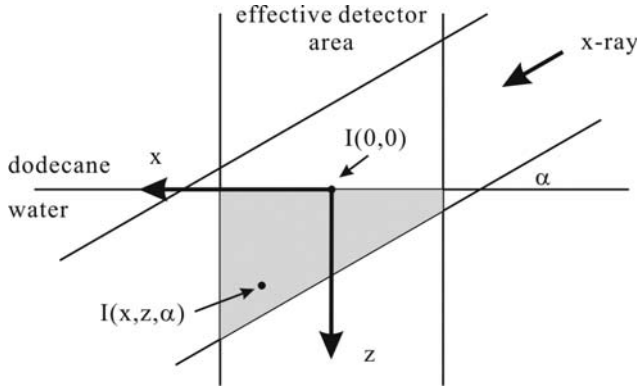

FIG. 4. Schematic diagram for the x-ray path, effective detector area, and the region of overlap in the bottom phase (shaded area).

upper phase. The expression in Eq. (1) is a good approximation under the assumption that variations of the salt concentration near the interface are weak and occur within a depth smaller than $\Lambda_w(\alpha)$. The $L\alpha$ emission line intensity from one Er^{3+} ion at the position (x,z) can be expressed as $I_{ion} \propto I(x,z,\alpha)e^{-\mu_{Er}(E)z}$, where the energy dependent $\mu_{Er}(E)$ is the absorption coefficient of the emission line in the bottom phase.

Integrating over the effective volume (the shaded area shown in Fig. 4) and assuming that the Er^{3+} concentration is uniform everywhere in the bottom phase allows the normalized fluorescence intensity, I/I_0, to be expressed as,

$$\frac{I}{I_0} = C\rho_{bulk}T(\alpha)\iint e^{-z/\tilde{\Lambda}(\alpha,E)}e^{\mu_0 z/\alpha}e^{-\mu_0 x}dxdz + C_s[1+R_F(Q_z)], \quad (2)$$

where ρ_{bulk} is the Er^{3+} bulk concentration, $\tilde{\Lambda}(\alpha,E) = \Lambda_w(\alpha)/[\Lambda_w(\alpha)\mu_{Er}(E)+1] \approx \Lambda_w(\alpha)$ because of the fact that $\Lambda_w(\alpha)\mu_{Er}(E) \ll 1$, and C is a scale factor that primarily depends upon the following features of the experimental setup: the collimator dimensions, the distance between the interface and Kapton window, and the ratio of $I(0,0) : I_0$. One should note that C also varies for different emission lines. For our experimental geometry, the integration along the y direction is constant and scales out in the data analysis. The second term in Eq. (2) represents the secondary scattering of the incident and reflected beams from the top phase, which is given approximately by the product of a proportionality constant, C_s, and the sum of the incident intensity represented by the factor "1" in Eq. (2), and the reflected beam intensity represented by the Fresnel reflectivity, $R_F(Q_z)$.

The solid lines in Fig. 3 are fits of the data obtained by varying the parameters C and C_s in Eq. (2). Here, $T(\alpha)$, $\tilde{\Lambda}(\alpha,E)$, and μ_0 are calculated based upon the data in Ref. 29. Small misalignments of the instrument are accounted for by an offset in Q_z ($= 4.0 \times 10^{-4}$ Å^{-1}, -4.0×10^{-4} Å^{-1}, and -1.1×10^{-4} Å^{-1} for the 0.01 M, 0.1 M, and 0.4 M $ErCl_3$ samples, respectively), which is responsible for the sharp feature at Q_c of the 0.01 M $ErCl_3$ sample appearing at a larger Q_z compared to the 0.1 M $ErCl_3$ sample. Although C_s cannot be directly measured, it is sensible to expect that the secondary scattering intensity below the critical angle should be close to the intensity at $Q_z = 0$ because the x-rays follow a similar path in both cases. For example, the best fit of the data from the 0.4 M $ErCl_3$ sample (squares in Fig. 3) yields $2C_s = 8.21 \times 10^{-6}$, while the $L\alpha$ intensity of the spectrum at $Q_z = 0$ (triangles in Fig. 2) is 8.26×10^{-6}.

The validity of the model in Eq. (2) is supported by the fact that the fits to the three different concentration samples yield a similar scale factor ($C = 2.48 \pm 0.15 \times 10^{-6}$ Å). This model assumed that the Er^{3+} concentration is uniform everywhere in the bottom phase; therefore, the high quality of the fits suggests that the concentration of Er^{3+} is not enhanced at the interface or that the enhancement is below the sensitivity of these measurements. We estimated the upper limit to this enhancement by fitting the data shown in Fig. 3 below the critical angle, where the signal is most sensitive to the interfacial structure, to a model consisting of Eq. (2) with an additional term: $C\sigma T(\alpha)\int e^{-\mu_0 x}dx$, where σ is the excess Er^{3+} interfacial concentration. This analysis used the same values of C and C_s previously obtained from the best fits shown in Fig. 3 to yield an upper limit on σ of approximately 1 Er^{3+} per 125 Å^2 to a statistical accuracy of two standard deviations.

B. Crud at the dodecane/water ($ErCl_3$) interface

An effective liquid-liquid extraction relies on the solubility of the metal complexes in their respective aqueous and organic phases.[30] A saturation and precipitation of the metal-ion complex from the organic (lighter) phase can result in the formation of a solid phase at the interface, commonly referred to as interfacial crud.[31] Cruds vitiate the separation and, from a practical perspective, need to be avoided. Although this is known to be a problem, there has been little work done to chemically or structurally characterize these precipitates, which may hold important clues to organic-phase metal-ion speciation. Here, we describe our initial application of the x-ray fluorescence near total reflection technique to characterize crud formation in a model solvent extraction system.

Crud formation in the existing system is studied by injecting 30.5 μL of HDEHP into the top phase of a dodecane/water (0.1 M $ErCl_3$) sample to produce an HDEHP concentration in the dodecane of about 10^{-3} M. Figure 5 shows the time course of the fluorescence spectrum monitored over several hours after the injection (time = 0 min). At this value of Q_z(= 0.008 Å^{-1}) the fluorescence primarily originates in the interfacial region. These data were measured before we incorporated the aluminum collimator into our experiment (see Fig. 1). As a result, the spectrum contains Cr ($K\alpha$) and Fe ($K\alpha$) peaks that are due to x-rays scattering from the stainless steel cap. The intensities of these extra peaks are time independent, whereas the intensity of the erbium emission lines increases with time. Visual observation of the sample revealed the presence of the formation of a macroscopically thick precipitate at the interface. These two observations

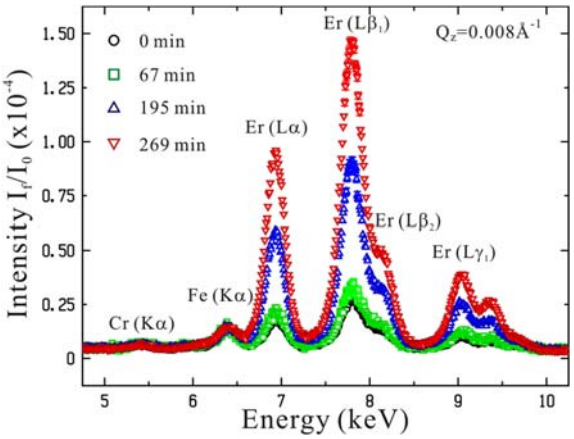

FIG. 5. (Color online) Fluorescence intensity measured at $Q_z = 0.008$ Å^{-1} (below the critical angle) for the dodecane (10^{-3} M HDEHP)/water (0.1 M $ErCl_3$) interface as a function of time after HDEHP was injected into the dodecane (at $t = 0$).

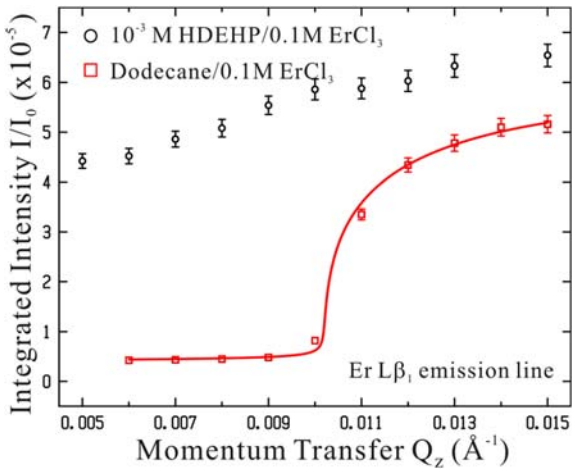

FIG. 6. (Color online) Er $L\beta_1$ emission line intensity vs the momentum transfer, Q_z for the dodecane (10^{-3} M HDEHP)/water (0.1 M $ErCl_3$) (circles) and the dodecane/water (0.1 $ErCl_3$) (squares) samples. The solid line is the best fit from Eq. (2).

imply that the formation of crud that contains Er^{3+} in the interfacial region is increasing with time.

This system reached equilibrium eight hours after the initial injection, as determined by a constant fluorescence intensity. The dependence of the fluorescence spectrum on Q_z was then measured. The variation of the $L\beta_1$ emission line intensity with Q_z is shown in Fig. 6. For comparison, the intensity from the neat interface without a collimator and its best fit (solid line) based on Eq. (2) are also shown in Fig. 6. Data from the system with crud (circles) are essentially linear with Q_z. Visual observation of the interface indicates that it is rough and inhomogeneous, consisting of many white domains whose size we estimate as between a few and hundreds of micrometers. Our inability to measure specular reflection from this interface is consistent with the visually observed roughness of the interface. These observations suggest that the fluorescence intensity primarily depends upon the depth of the penetration of x-rays into the thick interfacial layer of crud, which is linearly proportional to the small incident angles. Although further quantitative analysis of this set of data is not possible, more extensive experiments employing this methodology could be used to study the kinetics of crud formation.

IV. SUMMARY

The objective of this study was to develop the x-ray fluorescence technique to study liquid/liquid interfaces that are relevant to understanding solvent extraction. X-ray fluorescence near total reflection (XRNTR) was used to determine the Er fluorescence spectra from the interface between dodecane and aqueous solutions of $ErCl_3$. Quantitative analysis of data from samples with different $ErCl_3$ concentration yielded a unique scale factor, C, that accounts for the scattering geometry and is required to understand the Er^{3+} distribution at the interface. This analysis also indicated that the primary source of background fluorescence from ions in the lower aqueous phase is due to secondary scattering that originates in the dodecane phase. An upper limit of 1 Er^{3+} per 125 $Å^2$ (to an accuracy of 2 standard deviations) was placed on the enrichment of the interfacial Er^{3+}.

In addition, we have observed the formation of crud containing Er^{3+} at the interfacial region when HDEHP is present in the dodecane phase. Interfacial inhomogeneities in this particular system precluded a more quantitative analysis of the crud layer. However, the determination of a unique scale factor, C, will allow for the determination of metal ion adsorption during the course of a typical extraction in which crud does not form at the interface. We anticipate that XFNTR will be a useful tool for the study of metal ion enrichment from mixed salt solutions and for the determination of the coordination structure[23] of ions at oil/water and other liquid/liquid interfaces.[32]

ACKNOWLEDGMENTS

This work was supported by the U.S. DOE, OBES, Chemical Sciences, Geosciences, and Biosciences Division under Contract No. DE- AC02-06CH11357. M.L.S. acknowledges the Chemistry Division of the NSF for partial support of this work. ChemMatCARS (Sector 15) is supported by NSF Chemistry and DOE; the latter under the same contract. W.B. acknowledges Renato Chiarizia and Mark Jensen for assistance with the purification of HDEHP.

[1]*Interfacial Nanochemistry: Molecular Science and Engineering at Liquid-Liquid Interfaces*, edited by H. Watarai, N. Teramae, and T. Sawada (Plenum, New York, 2005).
[2]Y. R. Shen, Surf. Sci. **300**, 551 (1994).
[3]K. B. Eisenthanl, Chem. Rev. **96**, 1343 (1996).
[4]H. Nagatani, Z. Samec, P. F. Brevet, D. J. Fermín, and H. H. Girault, J. Phys. Chem. B **107**, 786 (2003).
[5]G. L. Richmond, Annu. Rev. Phys. Chem. **52**, 357 (2001).
[6]L. F. Scatena, M. G. Brown, and G. L. Richmond, Science **292**, 908 (2001).
[7]D. J. Fermín, Z. Ding, P. F. Breven, and H. H. Girault, J. Electroanal. Chem. **447**, 125 (1998).
[8]T. Osakai, H. Yamada, H. Nagatani, and T. Sagara, J. Phys. Chem. C **111**, 9480 (2007).
[9]L. T. Lee, D. Langevin, and B. Farnoux, Phys. Rev. Lett. **67**, 2678 (1994).
[10]B. R. McClain, D. D. Lee, B. L. Carvalho, S. G. J. Mochrie, S. H. Chen, and J. D. Litster, Phys. Rev. Lett. **72**, 246 (1994).
[11]D. M. Mitrinović, A. M. Tikhonov, M. Li, Z. Huang, and M. L. Schlossman, Phys. Rev. Lett. **85**, 582 (2000).
[12]T. Cosgrove, J. S. Phipps, and R. M. Richardson, Colloids Surf. **62**, 199 (1992).
[13]A. M. Tikhonov, S. V. Pingali, and M. L. Schlossman, J. Chem. Phys. **120**, 11822 (2004).
[14]M. K. Sanyal, V. V. Agrawal, M. K. Bera, K. P. Kalyanikutty, J. Daillant, C. Blot, S. Kubowicz, O. Konovalov, and C. N. R. Rao, J. Phys. Chem. C **112**, 1739 (2008).
[15]G. M. Luo, S. Malkova, J. Yoon, D. G. Schultz, B. H. Lin, M. Meron, I. Benjamin, P. Vanysek, and M. L. Schlossman, Science **311**, 216 (2006).
[16]P. R. Danesi, R. Chiarizia, and C. F. Coleman, Crit. Rev. Anal. Chem. **10**, 1 (1980).
[17]J. M. Bloch and W. B. Yun, Phys. Rev. A **41**, 844 (1990).
[18]W. B. Yun and J. M. Bloch, J. Appl. Phys. **68**, 1421 (1990).
[19]J. Daillant, L. Bosio, J. J. Benattar, and C. Blot, Langmuir **7**, 611 (1991).
[20]S. I. Zheludeva, N. N. Novikova, O. V. Konovalov, M. V. Kovalchuk, N. D. Stepina, and E. Yu, Mater. Sci. Eng., C **23**, 567 (2003).
[21]V. L. Shapovalov, M. E. Ryskin, O. V. Konovalov, A. Hermelink, and G. Brezesinski, J. Phys. Chem. B **111**, 3927 (2007).
[22]W. Bu and D. Vaknin, J. Appl. Phys. **105**, 084911 (2009).
[23]H. Tanida, H. Nagatani, and M. Harada, J. Phys.: Conf. Ser. **190**, 012061 (2009).
[24]L. Soderholm, S. Skanthakumar, and R. E. Wilson, J. Phys. Chem. A **113**, 6391 (2009).

[25]J. B. Roberto and T. Diaz de la Rubia, JOM **59**, 16 (2007).
[26]A. Goebel and K. Lunkenheimer, Langmuir **13**, 369 (1997).
[27]J. A. Partridge and R. C. Jensen, J. Inorg. Nucl. Chem. **31**, 2587 (1969).
[28]M. L. Schlossman, D. Synal, Y. Guan, M. Meron, G. Shea-McCarthy, Z. Huang, A. Acero, S. M. Williams, S. A. Rice, and P. J. Viccaro, Rev. Sci. Instrum. **68**, 4372 (1997).
[29]See http://henke.lbl.gov/optical_constants/ for information about calculation of these parameters.
[30]E. Paatero and J. Sjöblom, Hydrometallurgy **25**, 231 (1990).
[31]*Ion Exchange and Solvent Extraction of Metal Complexes*, edited by Y. Marcus and A. S. Kertes, (Wiley, New York, 1969), p. 715.
[32]V. A. Cocalia, M. P. Jensen, J. D. Holbrey, S. K. Spear, D. C. Stepinski, and R. D. Rogers, Dalton Trans. **11**, 1966 (2005).